Eric Ostovich ORCID iD: 0000-0001-9879-6913

Rebecca Klaper ORCID iD: 0000-0002-9239-6916

Title: Physiological Impacts of *Raphidocelis subcapitata* in Response to Lithiated Cobalt Oxide Nanomaterials

Title: Physiological Impacts of *Raphidocelis subcapitata* in Response to Lithiated Cobalt Oxide Nanomaterials

Authors: Eric Ostovich[1], Austin Henke[2], Curtis Green[2], Elizabeth Laudadio[2], Max Spehlmann[1], Nathan Van Ee[1], Jamie Uertz[3], Robert Hamers[2], Rebecca Klaper[1*]

[1]School of Freshwater Sciences, University of Wisconsin-Milwaukee, 600 E Greenfield Ave., Milwaukee, WI 53204

[2]Department of Chemistry, University of Wisconsin-Madison, 1101 University Ave., Madison, WI 53706

[3]CytoViva, Inc., 570 Devall Dr Ste 301 Auburn, AL 36832

* Corresponding author: rklaper@uwm.edu

Data Availability Statement: Data supporting this manuscript can be found online on a publicly available data repository with the following link: https://osf.io/qgtms/. Calculation tools such as R, ImageJ, and CellProfiler, are open-source tools available to anyone.

This article has been accepted for publication and undergone full peer review but has not been through the copyediting, typesetting, pagination and proofreading process, which may lead to differences between this version and the Version of Record. Please cite this article as doi: 10.1002/etc.5617.

Acknowledgments

This material is based upon the work supported by the National Science Foundation under Grant no. CHE-2001611, the NSF Center for Sustainable Nanotechnology. The CSN is part of the Centers for Chemical Innovation Program. Thanks to the Great Lakes Genomics Center and analytical chemistry labs at the University of Wisconsin-Milwaukee for use of equipment. The authors declare no conflicts of interest.

Author contributions:

Eric Ostovich: Conceptualization; Data curation; Formal analysis; Methodology; Visualization; Writing – original draft; Writing – review & editing. **Austin Henke:** Methodology; Resources. **Curtis Green:** Visualization. **Elizabeth Laudadio:** Data curation; Methodology; Resources; Writing – original draft. **Max Spehlmann, Nathan Van Ee:** Data curation; Writing – original draft. **Jamie Uertz:** Visualization; Writing – review & editing. **Robert Hamers:** Funding acquisition; Resources. **Rebecca Klaper:** Conceptualization; Funding acquisition; Methodology; Project administration; Supervision; Writing – review & editing

ABSTRACT

Complex metal oxide nanomaterials, like $LiCoO_2$ (LCO) nanosheets, are among the most widespread classes of nanomaterials on the market. Their ubiquitous application in battery storage technology drives their production to rates of environmental significance without sufficient infrastructure for proper disposal/recycling, thus posing a risk to ecosystem health and sustainability. This study assesses the general toxicological impacts of LCO when exposed to *Raphidocelis subcapitata*; physiological endpoints relating to growth and energy production are considered. Algal growth inhibition was significantly increased at concentrations as low as 0.1 μg·mL^{-1}, while exhibiting an EC_{50} of 0.057 μg·mL^{-1}. The average biovolume of cells were significantly enlarged at 0.01 μg·mL^{-1}, thus indicating increased instances of cell cycle arrest in LCO-treated cells. Additionally, LCO-treated cells produced significantly less carbon biomass while significantly overproducing neutral lipid content starting at 0.1 μg·mL^{-1}, thus indicating interference with CO_2 assimilation chemistry and/or carbon partitioning. However, the relative abundance of chlorophyll was significantly increased, likely to maximize light harvesting and compensate for photosynthetic interference. Cells that were treated with dissolved Li^{+}/Co^{2+} ions did not significantly impact any of the endpoints tested, suggesting LCO phytotoxicity is mainly induced through nano-specific mechanisms rather than ion-specific. These results indicate that this type of nanomaterial can significantly impact the way this algae proliferates, as well as the way it produces and stores its energy, even at lower, sublethal, concentrations. Furthermore, impairments to crucial cellular pathways, like carbon assimilation, could potentially cause implications at the ecosystem level. Thus, in future work, it will be important to characterize the molecular mechanisms of LCO at the nano-bio interface.

INTRODUCTION

As the field of nanotechnology continues to grow, and more consumer products start to incorporate nanomaterials into their design, understanding the environmental impacts of these nanomaterials is increasingly important. $LiCoO_2$ (LCO), for example, is a type of complex metal oxide nanosheet used as a cathode material for lithium ion batteries (Lu et al., 2014), which is found in many consumer electronics and high-end vehicles (Nitta, Wu, Lee, & Yushin, 2015). Increasing manufacturing rates, as well as a lack of infrastructure and economic incentive for recycling/disposal (Murphy, 2017) (Hamers, 2020) make LCO an emerging contaminant of concern. Since LCO contains high valence metals with unique catalytic properties, high reactivity, and known inherent toxicity, an accidental exposure of this type of nanomaterial could lead to many adverse outcomes.

Recent studies have begun to evaluate the general toxicological impacts of LCO exposure. For example, in *D. magna*, LCO has been found to reduce survival, rates of reproduction, and induce a differential expression in stress related genes (Bozich, Hang, Hamers, & Klaper, 2017); in RTgill-W1 cells, LCO has been seen to impact cell viability and cause significant production of ROS (Melby et al., 2018); and in *C. riparius*, LCO has been reported to cause delays in growth and development, as well as hinder the process of heme synthesis (Niemuth et al., 2019). However, more interestingly, LCO has also been reported to cause a number of molecular-level impacts. For example, in *D. magna*, there have been reports of an overwhelming disruption to energy metabolism related genes (Niemuth et al., 2021); in RTgill-W1 cells, there have been similar reports of significant overrepresentation in energy metabolism related pathways (Mensch et al., 2020); and in *C. riparius*, LCO has been reported to participate in redox reactions and alter the redox state of and Fe-S proteins, which are important for electron transfer, especially in energy metabolism related pathways (Niemuth et al., 2020). These findings are interesting because, at the molecular level, all three of these organisms are showing signs of impaired energy metabolism, and the significance of seeing this exact impairment in multiple organisms suggests that disruptions to energy related pathways may be a unifying molecular level impact of LCO across species. However, there are still many gaps in our knowledge as to the entirety of LCO's environmental consequences. Firstly, there has yet to be any data on the general toxicological impacts of algal species, whose crucial role in sustaining ecosystem health includes driving nutrient cycles and energy flow (Wang et al., 2019). Secondly, while we have some data to suggest that LCO interferes with pathways like glycolysis and respiration in animal-type organisms, we have no understanding as to how LCO may impact other pathways in primary producing-type organisms that are also tied to environmental processes, like photosynthesis.

The assimilation of CO_2, by primary producers, is necessary to support all life on Earth as consumers in the environment rely on this net primary production of carbon biomass as a source of chemical energy. More specifically, phytoplankton account for about half of the total global primary productivity with marine phytoplankton fixing around 50000 Tg CO_2 annually (Prasad et al., 2021), and freshwater phytoplankton fixing around an estimated 133 Tg CO_2 annually (Sayers et al., 2021). As such, a decrease in the efficiency of phytoplankton primary productivity could consequentially alter ecosystem energy budgets.

In this study, *Raphidocelis subcapitata,* a model algal bioindicator species (U.S. Environmental Protection Agency, 2012), was exposed to LCO for 48 hours. Several physiological endpoints were recorded in order to assess different aspects of cell fitness. Given our current understanding of the toxicological and molecular level impacts of LCO in other organisms, we hypothesize that LCO may negatively impact facets of algal physiology related to growth and energy production.

MATERIALS & METHODS

LCO Synthesis and Characterization.

Sheet-like nanoparticles of Li_xCoO_2 were synthesized using the techniques described in (Laudadio, Bennett, Green, Mason, & Hamers, 2018), (Laudadio, Ilani-Kashkouli, Green, Kabengi, & Hamers, 2019). Water with a resistivity 18.2 $M\Omega \cdot cm^{-1}$ was used for each step during the synthesis. A ($Co(OH)_2$) precursor was prepared using a precipitation reaction between LiOH and $Co(NO_3)_2 \cdot 6H_2O$. A 1 M $Co(NO_3)_2 \cdot 6H_2O$ was added drop-by-drop to a 0.1 M solution of LiOH. The precipitate was isolated and washed with 3 repeated cycles of centrifugation for 5 min at 4696 g as to isolate a pellet of particles, that was then resuspended in water. Next, the supernatant was removed after washing and the solid product was dried in a vacuum oven at 30 °C overnight. The $Co(OH)_2$ precursor was then lithiated to form Li_xCoO_2 by adding 0.20 g $Co(OH)_2$ particles to a molten salt flux of 6:4 molar ratio of $LiNO_3$:LiOH at 200 °C in a PTFE container equipped with magnetic stirring in a silicone oil bath. The particles were then heated and stirred in this molten salt flux for 30 min and the reaction was quenched with water. The precipitate was isolated and washed by 3 repeated cycles of centrifugation for 5 min at 4696 g to isolate a pellet of particles, which were then resuspended in water. Then the product was isolated from the supernatant and dried in a vacuum oven at 30 °C overnight.

The particles, digested in aqua regia, were analyzed using inductively coupled plasma – optical emission spectroscopy (ICP-OES) to yield a Li:Co ratio of 0.92:1. Surface area measurements, determined by nitrogen physisorption, yielded a surface area value of 125 $m^2 \cdot g^{-1}$. Powder X-Ray Diffraction yielded patterns consistent with previously published work which could be indexed to the $R\bar{3}m$ space group (found in **supplementary**

information). Individual LCO particles were imaged and sized using a FEI Tecnai T12 transition electron microscope where only particles completely captured in the image were measured. Thickness was measured of particles that appeared very dark as this means they were viewed edge-on. Length of particles were measured if clearly defined endpoints were visible and if it could reasonably be assumed that it was a single particle as opposed to an aggregate. Dynamic light scattering (DLS) and zeta potential measurements of LCO suspensions in algae media (found in **supplementary information**) were obtained with a Zetasizer Nano ZS Size Analyzer from Malvern Panalytical.

Algal Cell Culture.

A stock culture of *R. subcapitata* w, inoculated at 1×10^5 Cells·mL^{-1}, was cultured in a complete media comprised of Bold Modified Basal Medium (Sigma, B5282) and 18 MΩ water. Cells were illuminated with a full spectrum T8 light bulb at a continuous timescale. The stock solution was aerated with an aquarium air pump.

Exposure Setup.

This exposure was done to assess the impacts of LCO on *R. subcapitata* after 48 hours of exposure. Algae were exposed to one of four LCO concentrations or untreated control (0 μg·mL^{-1}, 0.01 μg·mL^{-1}, 0.1 μg·mL^{-1}, 1 μg·mL^{-1}, & 10 μg·mL^{-1} LCO), an ion control that contained the concentration of lithium and cobalt ions that would be present in the algae media containing 10 μg·mL^{-1} of LCO after 48 hours, and a dark control that was deprived of any light. In each treatment, done in quadruplicates, cells were seeded from the stock culture, after cells were growing exponentially, at 7×10^5 cells·mL^{-1} in T-25 flasks. A stock suspension of LCO was constituted in the algal complete media at 100 $\mu g \cdot mL^{-1}$. This suspension was sonicated for 25 minutes before the addition to respective samples to break up any aggregated nanoparticles. Additionally, an ion solution made from LiOH and $CoCl_2 \cdot H_2O$, also constituted in complete media, was made at 10X the concentration of ion dissolution of 10 $\mu g \cdot mL^{-1}$ of LCO after 48 hours. Dissolution of these particles was previously assessed using ICP-MS, where Li^+ was found to have a dissolution of 1024 $\mu g \cdot L^{-1}$ and Co^{2+} 239 $\mu g \cdot L^{-1}$ (Niemuth et al., 2019). For each treatment, complete media, LCO suspension, or 10X ion solution was added to 45 mL of cell suspension at a final volume of 50 mL. The samples were placed under full spectrum illumination at a photon flux of 70 $\mu E \cdot m^{-2} \cdot s^{-1}$, with the exception of the dark control samples, which were deprived of any light. At the conclusion of the exposure, the algal cells were spun down at 12000 x g for 7 minutes, and the media was aspirated. An additional vacuum centrifugation step was done to remove all moisture from the algae cell pellets that were used for elemental analysis.

Growth Inhibition.

Growth inhibition was measured as a first-line indicator of a toxicological response, as well as to determine the sensitivity of the algal cells to LCO (OECD, 2011). Before pelleting the algae samples, the cell concentration in each sample was determined by using optical density (OD) with an Agilent BioTek Synergy H4 Hybrid Microplate Reader at λ=680 nm. An OD_{680} was used since this microalgae absorbs light best at this wavelength. The absorptivity coefficient (found in **supplementary information**) was determined by plotting known concentrations of algae, determined with hemocytometry, against their respective absorbances. A 109 μL aliquot of each cell sample was placed in a well of a glass bottom 384 well plate (Cellvis, P384W-1.5H-N), which had a liquid height of 1 cm. Control samples were blanked with a solution of algae media while treated samples were blanked with an associated nanoparticle/ion control in order to account for the amount of light absorbance/scattering caused by the presence of LCO/ions in the medium. These nanoparticle/ion controls consisted of a suspension of LCO/Li^+ & Co^{2+} ions constituted in algae media that emulated the respective concentration of LCO/ions present in each treatment. Cell concentration values at T_0 and T_{48} were used to calculate growth rates and growth inhibition per OECD guidelines (OECD, 2011) as seen below, respectively:

$$\mu_{i-j} = \frac{\ln X_j - \ln X_i}{t_j - t_i} \; (day^{-1}) \text{ ………………………………(1)}$$

where μ_{i-j} represents the is the average specific growth rate from time i to j, X_i is the cell concentration at time i, and X_j is the cell concentration at time j;

$$\%I_r = \frac{\mu_C - \mu_T}{\mu_C} \times 100 \text{ ………………………………...(2)}$$

where $\%I_r$ represents the percent inhibition in average specific growth rate, μ_C is the mean value for average specific growth rate (μ) in the control group, and μ_T is the average specific growth rate for the treatment replicate. An EC_{50} value, based on the growth inhibition data, was statistically determined with a three-parameter log-logistic model using the drc package in R (Ritz & Strebig, 2016).

Biovolume.

Biovolume, which can be described as the volumetric space occupied by an algal cell, is a morphological trait that was used as a simple measurement of phenotypic change to the cell. Alterations to the biovolume of microalgae can have an impact on its functional properties like access to nutrients and light, velocity of sinking, and tolerance to grazing (Borics et al., 2021), however, in the case of *R. subcapitata*, it can also be an indication of disruption to cell cycle progression (Machado & Soares, 2020). Cell samples from each treatment were imaged with an EVOS™ XL Core Imaging System, equipped with an EVOS™ 40X LWD achromatic phase contrast objective. Cell images were processed in ImageJ to estimate single cell dimensions using methods described by (Esra Dökümcüoğlu & Yılmaz, 2020). Biovolumes of individual algal cells were calculated as described by (Machado & Soares, 2014) with the assumption that *R. subcapitata* is generally shaped like a sickle-shaped cylinder (Sun & Liu, 2003) per the following equation:

$$V = \frac{\pi}{6} \cdot l \cdot w^2 \ldots\ldots\ldots\ldots\ldots\ldots\ldots\ldots\ldots\ldots\ldots\ldots \text{(3)}$$

where V represents the biovolume of the cell, l is the length of the cell, and w is the transapical width of the cell. At least 100 cells were analyzed from each independent sample and were averaged, and then the average values for all independent samples were averaged by treatment to obtain the average biovolume value.

Elemental Analysis.

Dried algae pellet samples were accurately weighed into small tin cups on a microbalance. Sample filled tin cups were crushed into small spheres that could be inserted into the EA's auto sampler. Samples dropped, one at a time, from the rotating auto sampler into the combustion column where they were converted into simple gases (e.g. CO_2, H_2, N_2). Unwanted materials such as halogens, sulfur, phosphorous, NOx, and excess oxygen from combustion were removed with Cu, CrO_3, CoO, $Mg(Cl_4)_2$, and NaOH reagents in the oxidation/reduction chamber. From there, elements were separated by gas chromatography (GC) with a helium carrier gas before passing by a thermal conductivity detector.

Post run analyses started by investigating the retention time (RT) of each sample. The RT is the amount of time in decimal minutes between sample injection and chromatogram peak. Because the EA uses GC, the RT is directly related to the molecular weight (MW) of the simple gas, which in this case was used to estimate the amount of carbon present in each algae sample. Acetanilide standards were used to construct a calibration curve.

Net production of Carbon Biomass.

The net production of carbon biomass was recorded as a measurement of net primary productivity. The total amount of carbon in each sample was calculated using the carbon peak areas measured by the EA and in reference to the acetanilide standard curve. Then the amount of carbon per cell was calculated by dividing the amount carbon in the sample by the number of cells from the pellets present in each respective sample. The net production of carbon biomass produced per cell for each sample was then calculated using the following equation:

$$NCP = \left(\frac{Mass\ C_{Sample}}{\#cells_{Sample}}\right) - \bar{x}\left(\frac{Mass\ C_{Dark}}{\#cells_{Dark}}\right) \ldots\ldots\ldots\ldots\ldots\ldots\ldots\ldots(4)$$

Where NCP represents net carbon biomass produced per cell, $Mass\ C_{Sample}$ is the mass of carbon in any given sample, $\#cells_{Sample}$ represents the number of cells in any given sample determined through OD, $Mass\ C_{Dark}$ is the mass of carbon specifically in the dark controls, and $\#cells_{Dark}$ is the number of cells specifically in the dark controls. The mass of carbon per cell for each sample was subtracted by the average mass of carbon per cell from the dark controls, as they theoretically should not have produced any carbon biomass without a light source, thus yielding a net production in carbon biomass per cell value for each sample. NCP values were then further normalized to the average biovolume in each sample as a means to correct for changes in cell size.

Neutral Lipid Content.

Neutral lipid content was measured as an additional stress response since these lipid droplets tend to accumulate downstream of certain stressors and/or nutrient depravation in microalgae and can be indicative of impairments to energy metabolism (Bellou & Aggelis, 2012). To assay for neutral lipid content, cells were stained post exposure with BODIPY™ 505/515, which selectively binds to neutral lipids. $1{\times}10^6$ cell aliquots were obtained from each sample and transferred to sterile microcentrifuge tubes, where additional algal complete media was added at a final volume of 1 mL. BODIPY™ was then added to each sample at a final concentration of 5 µM, including a no-cell control with only complete media, whereafter samples were incubated in darkness at room temperature for 15 minutes. 100 mL aliquots were transferred to a glass bottom 384 well plate (Cellvis, P384W-1.5H-N) and fluorescence measurements were then taken on an Agilent BioTek Synergy H4 Hybrid Microplate Reader at an excitation and emission wavelength of 470/20 nm and 540/20 nm, respectively. Relative lipid content was calculated by taking the difference of the average no-cell control and respective sample RFU values and then normalizing to the corrected non-treated cell control RFU values.

Additionally, cells were also imaged with an EVOS™ M7000 Imaging System to visualize the lipid droplets as a qualitative assessment of neutral lipid content.

Single-Cell Chlorophyll Fluorescence Microscopy.

100 µL aliquots from each sample were plated in to a well of a glass bottom 384 well plate (Cellvis, P384W-1.5H-N) and spun gently at 600RPM for 1 minute to concentrate cells at the bottom of the well. Cells were then dark adapted for 30 min before imaging with an ImageXpress Micro XLS High-Content Screening System. For image acquisition, cells were visualized using a Cy 5 filter (ex/em: 628/692), thereby exciting chlorophyll molecules, and a 60X Plan Fluor 0.85 NA objective (Molecular Devices, 1-6300-0414); 16 sites per well were acquired. For representative cell figures, images were also acquired with a 100X CFI L PLAN EPI CC 0.85 NA objective (Molecular Devices, 1-6300-0419) for better resolution. After acquiring images, bioimage analysis was conducted with CellProfiler [v4.2.1, (Stirling et al., 2021)] for segmenting images and measuring the respective fluorescence intensities of individual cells. The average "mean_cell_intensity" values from each treatment were used to represent the relative abundance of chlorophyll content.

Enhanced Dark-Field Hyperspectral Imaging.

To confirm cellular uptake of LCO, algal samples were analyzed using the CytoViva Enhanced Darkfield Hyperspectral System, which uses patented darkfield optics to generate high contrast, high signal-to-noise ratio images. These images were scanned via the CytoViva HSI system using a spectrograph that captures the entire field of view in which each pixel of the image contains hyperspectral data from 400-1000nm. Samples were placed on a glass slide and imaged with a 100x oil immersion objective. A reference spectral library for LCO was created by collecting spectral data from a suspension of LCO and then searching algal samples that had been exposed to 1 $\mu g \cdot mL^{-1}$ LCO. The spectral analysis was done using the ENVI software to identify the presence of LCO particles associated with the algal cells, and the Spectral Angel Mapping algorithm was used to show the presence of the particles.

Statistical Analysis.

Statistical analyses were performed using R Studio (R Core Team, 2019; RStudio Team, 2020). A Shapiro-Wilk test was performed to determine whether the respective data sets were normally distributed, and a One-Way ANOVA with a Tukey post-hoc test was used to compare the means of normally distributed data. A non-parametric Kruskal-Wallis test with a Dunn's post-hoc test was used to compare the means of non-normally distributed data. In each case, a 95% confidence interval was used to determine significant differences within a data set. Additionally, to compare growth inhibition results to biovolume results, a Pearson coefficient was constructed using R Studio.

RESULTS

LCO Characterization.

LCO is a type of complex metal oxide nanomaterial with a sheet-like morphology comprised of intercalating layers of lithium and cobalt oxide. TEM sizing of single LCO particles suggests an average thickness and length of 5.54 ± 2.01 nm and 39.63 ± 17.35 nm, respectively (**Figure 1**). The zeta-potential values for LCO suspended in algal complete media indicate that this nanomaterial is highly negatively charged at higher concentrations like 1 μg·mL^{-1} (−22.73 mV) and 10 μg·mL^{-1} (−30.33 mV), while becoming much less negatively charged at lower concentrations like 0.1 μg·mL^{-1} (-10.07 mV) and 0.01 μg·mL^{-1} (-2.01 mV). These results suggest that there's an increasing degree of repulsion between LCO nanoparticles with increasing concentrations (Samimi, Maghsoudnia, Eftekhari, & Dorkoosh, 2018), and since electrostatic repulsion is one of the primary sources of nanomaterial stability in aqueous media, this would indicate that LCO, in theory, is increasingly stable at higher concentrations when suspended in the complete media and therefore less prone to forming aggregates at those concentrations (Afshinnia et al., 2019). However, in practicality, this isn't necessarily the case as visible aggregates can be seen in treatments as low as 1 μg·mL^{-1} post exposure, which indicates a lack of stability. Furthermore, it's worth noting that in other types of exposure media like MHRW, LCO also tends to aggregate and settle as well, thus lacking stability in suspension (Niemuth et al., 2019).

Growth Inhibition and Biovolume.

The level of growth inhibition experienced by LCO-treated cells increased in a dose dependent manner, with significantly higher levels of growth inhibition in comparison to the control at concentrations as low as 0.1 μg·mL^{-1}.(**Figure 2a**). This is a first-line indicator that LCO induces a toxicological stress response on these algal cells that either causes a decrease in cellular proliferation or an increase in cell death. Furthermore, based on the growth inhibition data, the EC_{50} was calculated to be around 0.057 μg·mL^{-1}. In the control, cells had an average biovolume of about 22 μm^3, which is consistent with what's reported in the literature for normal biovolumes of this cell type (Machado & Soares, 2014). However, the average biovolume seems to also increase in a dose dependent manner with significant increases to cell size at concentrations as low as 0.01 $\mu g \cdot mL^{-1}$ (**Figure 2b**). These larger biovolumes, while only a direct measurement of cell morphology, may indicate a more serious issue in terms of cell health. *R. subcapitata* cells go through several stages of their cell cycle in which they increase in size, replicate their nuclei, and release multiple, smaller, daughter cells (**Figure 2c**). An increase in the average biovolume may indicate cell cycle interruption/arrest (Machado & Soares, 2020). This is because, for this type of algae, cells that have lost the ability to proliferate, or divide into multiple daughter cells, may still be able to increase in size and/or replicate their nuclei (depending on the cell cycle stage of arrest) as if they were going to proliferate, thus leading to an overall increased average biovolume observed in said populations. When comparing growth inhibition to biovolume, there’s an extremely high Pearson correlation between the level of growth inhibition experienced and the average size of algal cells, thus perpetuating the idea that LCO may impact cell cycle progression (**Figure 2d**). This makes sense as inhibitory effects on growth and cell cycle progression would go hand-in-hand. Increased levels of growth inhibition could potentially also be attributed to an increase in senescence, however, assays that directly measure cell death would be needed to validate this prospect. Interestingly, no significant differences in growth inhibition nor biovolume were observed in ion treated cells, this suggesting that LCO induced phytotoxicity is initiated through nano-specific mechanisms, rather than ion-specific mechanisms like in the bacterium, *Shewanella oneidensis* (Hang et al., 2016).

Net Carbon Production.

Unlike growth inhibition and biovolume, the net production of carbon biomass produced per cell did not change with respect to concentration in a dose-dependent manner (**Figure 3**). Control cells obtained a net average production of 0.078 pg $C \cdot Cell^{-1} \cdot \mu m^{-3}$ while LCO-treated cells, in comparison, had only produced roughly 50% less across the board with significant reductions at concentrations as low as 0.1 $\mu g \cdot mL^{-1}$. These results suggest that even at lower, sublethal, concentrations, LCO induces massive reductions to the net production of carbon biomass in these cells. These reductions may result from an increased inactivation of photosynthetic machinery, thus leading to an overall decrease in CO_2 assimilation (Antal, Krendeleva, & Tyystjärvi, 2015); they may also result from an increase in glycolytic activity which has been reported in several other organisms in response to LCO exposure (Mensch et al., 2020), (Niemuth et al., 2020), (Niemuth et al., 2021). Even more likely, however, may be a combination of both as an imbalance between carbohydrate production and carbohydrate consumption. Either way, since entire food webs are dependent on primary producing organisms to drive nutrient cycles and energy flow in freshwater ecosystems (Wang et al., 2019), this is concerning as widespread contamination of LCO could possibly mean largescale restructuring of ecosystem dynamics and energy budgets.

Neutral Lipid Content.

Microalgae are known for their ability to produce large quantities of neutral lipids called Triacylglycerol, or TAG, and its biosynthesis is largely thought to serve as an energy store, much like starch (Johnson & Alric, 2013). Under optimal conditions, microalgae don't actually produce very much TAG as it's a less preferred form of carbon storage compared to starch, but when they're subject to certain stressors and nutrient deprivation, it causes them to significantly increase their TAG content. Most notably, *Chlamydomonas reinhardtii* has been shown to significantly increase TAG production in response to nitrogen starvation (Harchouni, Field, & Menand, 2018). When exposed to these stressors, there ends up being a shift in their metabolism that favors the production and accumulation of TAG over starch, however, the reasoning behind this is not quite clear (Battah, El-Ayoty, Abomohra, El-Ghany, & Esmael, 2015). Although, since fatty acids have a higher energy/mass ratio with a higher energy return upon fatty acid oxidation (almost 6.7 ATP equivalents per C) compared to glucose oxidation (about 5.3 ATP equivalents per C), TAG accumulation may be more beneficial in times of energy starvation/ATP deficiencies (Johnson & Alric, 2013). TAG accumulation is also especially present in quiescent cells, which are cells that aren’t actively dividing, but their photochemistry is still active to some extent (Ischebeck, Krawczyk, Mullen, Dyer, & Chapman, 2020).

As displayed in **Figure 4a**, a representative fluorescence micrograph depicts a control cell (top), containing a minimal amount TAG content, in comparison to an LCO-treated cell (bottom, 1 $\mu g \cdot mL^{-1}$) which has produced a seemingly larger amount of TAG. Further validating this observation, the microplate assay results in **Figure 4b** roughly exhibit a positive correlation between LCO concentration and relative neutral lipid content. A significant peak production is seen at 1 $\mu g \cdot mL^{-1}$ of LCO with over a 100% increase in TAG content compared to the control. However, once again, no significant increase in TAG production was observed in ion treated cells. These results suggest that LCO exposure leads to a metabolic shift in these cells which favors the production and accumulation of TAG over starch, and thus may be indicative of an interference to their energy and central carbon metabolism (Bellou & Aggelis, 2012). One factor leading to this increase in TAG production may be due to the presence of Co^{2+} in LCO. Other algal species like *Chlorella vulgaris*, for example, have been reported to increase their production of TAG when exposed to heavy metals like cobalt (Battah et al., 2015). Although, in this case, this would only be true for Co^{2+} in the nano form, as opposed to the ionic from.

Single-Cell Chlorophyll Fluorescence Microscopy.

High-content fluorescence imaging was firstly used to visually inspect LCO-induced changes to cell morphology. The morphology of LCO-treated cells (**Figure 5c-d**) appear larger in size compared to the control cell (**Figure 5a**), aligning with results in **Figure 2b**. LCO-treated cells also appear to have more of a “French croissant”-type shape (**Figure 5d**), similar to that of algae cells exposed to metolachlor, as described by Machado & Soares, 2020. Other 2D nanomaterials, like graphene-oxide, have previously been reported to elicit mechanical disturbances to the cell by damaging the membrane with their sharp edges (Malina et al., 2019). However, when comparing the morphology of LCO-treated cells to that of the Carfentrazone-treated cell (**Figure 5b**), used as a positive control for membrane damage (Li et al., 2003), their morphologies appear quite different. While the LCO-treated cells look larger and brighter compared to the control, they still appear to uphold the structural integrity of their membrane. By contrast, the morphology of the membrane damaged positive control appears to have lost its structural integrity while displaying more of a “stringed pearls”-type shape. Furthermore, high-content fluorescence imaging and bioimage analysis were also employed to quantify the emitted fluorescence intensities of individual cells, which are proportional to the abundance of chlorophyll within those cells. LCO-treated cells appear to have higher fluorescence intensities, and thus increased chlorophyll content, relative to the control, with significant increases at 0.1 & 1 $\mu g \cdot mL^{-1}$ LCO (**Figure 5e**). This is contrary to other types of metal oxide nanomaterials which have been reported to decrease chlorophyll content (Saxena & Harish, 2018). However, in the event of photosynthetic inhibition, cells are likely to produce more chlorophyll to maximize light harvesting (Vieira et al., 2017).

Enhanced Dark-Field Hyperspectral Imaging

Enhanced dark-field microscopy coupled with hyperspectral imaging was employed to visualize the interactions of LCO particles with the algal cells. LCO deposits, visible as white pockets of scattered light, can be seen internalized within the LCO-treated cells (**Figure 6f**). These LCO deposits are only visible on the same Z-focal plane as the cells (i.e., not above or below) and are not seen on their outer perimeter, thus suggesting that LCO actually enters the cells rather than just adhering to the outer surface. No LCO deposits were identified within the control cells (**Figure 6c**). A spectral reference library for LCO was constructed using a samples of LCO particles in algae media and samples of LCO-treated algae (**Figure 6a**). The spectral angle mapping algorithm identified pixels, mapped in red, that matched the LCO spectra, thus verifying the presence of LCO deposits in the LCO-treated algal cells (**Figure 6g**). As expected, these spectra were not identified in the control cells, and therefore no mappings were generated (**Figure 6d**). The mechanism of internalization is unclear, however the vesicular shape of the tightly packed LCO deposits (**Figure 6f**) may suggest uptake through endocytosis. Yan et al., 2021 reported that the uptake of AIE functionalized Ag nanoparticles, with a similar zeta-potential and aggregational behavior to LCO, were mediated through clathrin-dependent endocytosis.

DISCUSSION

To investigate the fitness of *R. subcapitata* in response to LCO, several endpoints tied to growth and energy production were evaluated. Each of the parameters tested are metabolically related to one another and can influence larger ecosystem outcomes. For example, the amount of net carbon biomass produced by individual cells will determine how much energy is available to sustain their routine cell maintenance. And should the cells become energy deficient, they may not be able to sustain energy intensive processes like cell division, thus causing them to enter a state of quiescence. Cells in this sort of state could foster larger biovolumes as they would've lost the ability to proliferate, and to accumulate neutral lipids like TAG due to a shift in their central carbon metabolism. Ultimately, this would also lead to a decline in phytoplankton communities. And then over time, with a reduction in the amount of carbon biomass being produced per cell, and with diminished phytoplankton availability in general, this could significantly alter ecosystem energy budgets.

In this experiment, as hypothesized, facets of algal physiology related to growth and energy production were negatively impacted in response to LCO. Negative impacts to growth were exhibited by a significant increase in growth inhibition and biovolume, which indicates an increase in cell cycle disturbances. Negative impacts to energy production were exhibited by a significant decrease in the net production of carbon biomass, as well as a significant overproduction of TAG, which indicates interference with CO_2 assimilation chemistry and/or carbon partitioning. Relative chlorophyll content, however, was significantly increased. While increased chlorophyll content could be considered an enhancement to photosynthesis, as argued by Zhang et al., 2021, this may be more indicative of a compensatory action to increase light harvesting in this case as the amount of carbon biomass was still negatively impacted. Interestingly, though, cells that were treated with dissolved Li^+/Co^{2+} ion controls did not significantly impact any of the endpoints tested, which suggests that LCO phytotoxicity is mediated through nano-specific mechanisms rather than ion-specific. The reason for this is unclear, especially since engineered nanoparticles tend to behave unpredictably in complex biological media. However, with its unique physiochemical properties and high surface area-to-volume ratio, it's possible that LCO could obtain certain surface modifications/protein coronas in its nano form that make it interact more favorably with cells in comparison to it's ionic form (Dai et al., 2018).

These responses clearly demonstrate the adverse impacts of LCO on the physiology of *R. subcapitata* and suggest a likely disruption of key metabolic processes relating to cell growth and energy production/metabolism. One possible mechanism that may initiate the observed toxicological responses is the likely ability of LCO to participate in redox reactions, especially with iron containing proteins, as it was determined in *C. riparius* (Niemuth et al., 2021). This could also be possible for algae as cellular uptake of LCO nanoparticles was observed with enhanced dark-field hyperspectral imaging.

In study by Niemuth et al., 2019 found *Chironomus riparius* exposed to LCO had a significantly decrease in the function of the iron-containing protein, hemoglobin. This was supported both quantitatively from green absorbance and qualitatively from the loss of their deep red color to a pale-yellow color (their natural red color is due to the presence of heme proteins). This is concerning as proteins with heme and iron-sulfur centers are important for the transfer of electrons in many essential life processes like respiration, and in the case of algae, photosynthesis as well (Atamna, Walter, & Ames, 2002).

One such protein with an iron-sulfur center involved in the process of photosynthesis is Ferredoxin. In a study done by Isabel and José Moura, they were able to use EPR to prove that in the Ferredoxin II protein from *Desulfovibrio gigas*, cobalt was able to be incorporated into the vacant site of the iron-sulfur cluster, thus reducing it to a $CoFe_3S_4$ cluster (Moura, Moura, Münck, Papaefthymiou, & LeGall, 1986). It's possible that similar phenomena could be happening with the cobalt from the LCO, in which case causing a conformational change in those iron-sulfur proteins that change their overall chemistry. This could be especially harmful to the function of the iron-sulfur proteins involved in respiration and photosynthesis as they must remain in an oxidized state to be able to accept and transfer electrons in their respective electron transport chains, which is needed to produce ATP, as well as NADPH in photosynthesis. Since life is dependent on the movement of electrons, a short in this biochemical circuit could reduce the efficiency of the cell's ability to carry out life processes like photosynthesis, which would help explain the decreased net production of carbon biomass, as well as the increase in growth inhibition for LCO-treated cells.

Heavy metal contaminants, in general, have been seen to inhibit primary productivity in aquatic environments (Kaladharan et al. 1990). However, cobalt itself has been reported to decrease the growth of green algae at concentrations as low as 0.6 $\mu g \cdot mL^{-1}$ (H.Kim, J.; J.Gibbs, H.; D.Howe, P.; Wood, 2006), (Horvatić et al. 2007), (El-Sheekh et al.2003).

Additionally, cobalt has also been reported to decrease the amount of O_2 evolution in green algae at certain concentrations, and has been seen to directly target PSII, meaning that cobalt can and does interfere with electron transport and photosynthetic efficiency (Horvatić et al., 2007), (El-Sheekh et al., 2003). This further supports the idea that the cobalt from LCO could be an initiator for adverse outcomes observed in eukaryotic organisms that have been exposed to this type of nanomaterial (Niemuth et al., 2019).

Other 2D-nanomaterials like graphene-oxide, have been reported to have different, physical, mechanisms of toxicity relating to membrane damage, nutrient depletion, and by covering the surface of, and therefore shading, the cell (Malina et al., 2019). In terms of membrane damage and cell surface covering, these occurrences were proven to not be the case for LCO through microscopic observation. Fluorescence imaging showed a discrepancy between the morphology of LCO-treated cells and membrane damaged positive control cells, thus suggesting that LCO does not cause membrane damage. Additionally, enhanced dark-filed hyperspectral imaging revealed that while cells were internalizing LCO nanoparticles, they were not simply adhering to/covering the surface of the cell, thus indicating that light This makes sense as the surface charge of LCO and cell membranes are electrostatically incompatible. For example, Kim et al., 2022 reported with QCM-D that negativley charged nanodots do not interact/adhere to negatively charged plant bio-surfaces due to electrostatic incompatibilities. But in terms of nutrient depletion, LCO has been reported to adsorb nutrients like phosphate (Laudadio et al., 2019), which could, in theory, partially explain some of the disturbances. However, in cases of nutrient depletion, algae also typically undergo chlorosis as they are related to one another (Yaakob et al., 2021). Not only was this not the case for LCO-treated cells, but the opposite trend was actually observed, thus suggesting that nutrient depletion is not a major factor for LCO-induced toxicity in algae.

Overall, LCO significantly alters different aspects of *R. subcapitata* physiology even at lower, sub lethal, concentrations, and therefore may also likely pose a risk to other types of phytoplankton as well. Most concerning is LCO's impact to algal growth and net primary productivity, which could have several ecologically related implications. Primarily, altering the efficiency of phytoplankton productivity could impact the sustainability of freshwater ecosystems. Thus, widespread contamination of LCO to freshwater ecosystems would likely limit the amount of nutrients and chemical energy needed to support all life in those systems by decreasing the density of phytoplankton communities and their associated productivity at the cellular level.

CONCLUSION

As engineered nanomaterials continue to grow in use and production, it will be important to have a better understanding as to how they will interact with the environment and what effects they'll have on ecosystem health. Here we provide insight into the initial impacts of LCO nanosheets on the microalgae, *R. subcapitata*. Physiological impacts observed in this work indicate that LCO significantly alters the way this algae proliferates, and the way it produces and stores its energy, thus leading to an overall decrease in the amount of useful chemical energy it's able to provide to aquatic food web networks. However, additional efforts should be spent to assess the cellular and molecular mechanisms that govern these physiological impacts.

These impacts, while assessed at the cellular level, may have larger ecosystem level implications as freshwater ecosystems are entirely reliant on the ability of primary producing organisms like, like *R. subcapitata*, to drive nutrient cycles and energy flow. Thus, in the future, it will be important for us to develop infrastructure for the proper and sustainable storage or recycling of this type of engineered nanomaterial as a means to prevent its widespread contamination.

REFRENCES

Afshinnia, K., Sikder, M., Cai, B., Carolina, S., Carolina, S., Carolina, S., … Carolina, S. (2019). Effect of nanomaterial and media physicochemical properties on Ag NM aggregation kinetics. *Journal of Colloid and Interface Science*, 1–31.

Antal, T. K., Krendeleva, T. E., & Tyystjärvi, E. (2015). Multiple regulatory mechanisms in the chloroplast of green algae: Relation to hydrogen production. *Photosynthesis Research*, *125*(3), 357–381. https://doi.org/10.1007/s11120-015-0157-2

Atamna, H., Walter, P. B., & Ames, B. N. (2002). The role of heme and iron-sulfur clusters in mitochondrial biogenesis, maintenance, and decay with age. *Archives of Biochemistry and Biophysics*, *397*(2), 345–353. https://doi.org/10.1006/abbi.2001.2671

Battah, M., El-Ayoty, Y., Abomohra, A. E. F., El-Ghany, S. A., & Esmael, A. (2015). Effect of Mn2+, Co2+ and H2O2 on biomass and lipids of the green microalga Chlorella vulgaris as a potential candidate for biodiesel production. *Annals of Microbiology*, *65*(1), 155–162. https://doi.org/10.1007/s13213-014-0846-7

Bellou, S., & Aggelis, G. (2012). Biochemical activities in Chlorella sp. and

Nannochloropsis salina during lipid and sugar synthesis in a lab-scale open pond simulating reactor. *Journal of Biotechnology*, *164*(2), 318–329. https://doi.org/10.1016/j.jbiotec.2013.01.010

Borics, G., Lerf, V., T-Krasznai, E., Stanković, I., Pickó, L., Béres, V., & Várbíró, G. (2021). Biovolume and surface area calculations for microalgae, using realistic 3D models. *Science of the Total Environment*, *773*. https://doi.org/10.1016/j.scitotenv.2021.145538

Bozich, J., Hang, M., Hamers, R., & Klaper, R. (2017). Core chemistry influences the toxicity of multicomponent metal oxide nanomaterials, lithium nickel manganese cobalt oxide, and lithium cobalt oxide to Daphnia magna. *Environmental Toxicology and Chemistry*, *36*(9), 2493–2502. https://doi.org/10.1002/etc.3791

Dai, Q., Bertleff-Zieschang, N., Braunger, J. A., Björnmalm, M., Cortez-Jugo, C., & Caruso, F. (2018). Particle Targeting in Complex Biological Media. *Advanced Healthcare Materials*, *7*(1), 1–32. https://doi.org/10.1002/adhm.201700575

El-Sheekh, M. M., El-Naggar, A. H., Osman, M. E. H., & El-Mazaly, E. (2003). Effect of cobalt on growth, pigments and the photosynthetic electron transport in Monoraphidium minutum and Nitzchia perminuta. *Brazilian Journal of Plant Physiology*, *15*(3), 159–166. https://doi.org/10.1590/S1677-04202003000300005

Esra Dökümcüoğlu, V., & Yılmaz, M. (2020). Assessment of Cell Counting Method Based on Image Processing for a Microalga Culture. *MedFAR*, *3*(2), 75–81. Retrieved from https://www.researchgate.net/publication/341792505_Assessment_of_Cell_Countin g_Method_Based_on_Image_Processing_for_a_Microalga_Culture

H.Kim, J.; J.Gibbs, H.; D.Howe, P.; Wood, M. (2006). Concise International Chemical Assessment Document 69: Cobalt and Inorganic Cobalt Compounds. *World Health Organization*, 1–93. Retrieved from http://www.who.int/ipcs/publications/cicad/cicad70.pdf

Hamers, R. J. (2020). Energy storage materials as emerging nano-contaminants. *Chemical Research in Toxicology*, *33*(5), 1074–1081. https://doi.org/10.1021/acs.chemrestox.0c00080

Hang, M. N., Gunsolus, I. L., Wayland, H., Melby, E. S., Mensch, A. C., Hurley, K. R., … Hamers, R. J. (2016). Impact of Nanoscale Lithium Nickel Manganese Cobalt Oxide (NMC) on the Bacterium Shewanella oneidensis MR-1. *Chemistry of Materials*, *28*(4), 1092–1100. https://doi.org/10.1021/acs.chemmater.5b04505

Harchouni, S., Field, B., & Menand, B. (2018). AC-202, a highly effective fluorophore for the visualization of lipid droplets in green algae and diatoms. *Biotechnology for Biofuels*, *11*(1), 1–9. https://doi.org/10.1186/s13068-018-1117-9

Horvatić, J., Peršić, V., Pavlić, Ž., Stjepanović, B., & Has-Schön, E. (2007). Toxicity of metals on the growth of Raphidocelis subcapitata and Chlorella kessleri using microplate bioassays. *Fresenius Environmental Bulletin*, *16*(7), 826–831.

Ischebeck, T., Krawczyk, H. E., Mullen, R. T., Dyer, J. M., & Chapman, K. D. (2020). Lipid droplets in plants and algae: Distribution, formation, turnover and function. *Seminars in Cell and Developmental Biology*, *108*(February), 82–93. https://doi.org/10.1016/j.semcdb.2020.02.014

Johnson, X., & Alric, J. (2013). Central carbon metabolism and electron transport in chlamydomonas reinhardtii: Metabolic constraints for carbon partitioning between oil and starch. *Eukaryotic Cell*. https://doi.org/10.1128/EC.00318-12

Kaladharan, P., Pillai, V. K., & Balachandran, V. K. (1990). Inhibition of Primary Production As Induced By Heavy Metal Ions on Phytoplankton Population Off Cochin, *37*(1), 51–54.

Kim, K., Jeon, S. J., Hu, P., Anastasia, C. M., Beimers, W. F., Giraldo, J. P., & Pedersen, J. A. (2022). Sulfolipid density dictates the extent of carbon nanodot interaction with chloroplast membranes. *Environmental Science: Nano*, *9*(8), 2691–2703. https://doi.org/10.1039/d2en00158f

Laudadio, E. D., Bennett, J. W., Green, C. M., Mason, S. E., & Hamers, R. J. (2018). Impact of Phosphate Adsorption on Complex Cobalt Oxide Nanoparticle Dispersibility in Aqueous Media. *Environmental Science and Technology*, *52*(17), 10186–10195. https://doi.org/10.1021/acs.est.8b02324

Laudadio, E. D., Ilani-Kashkouli, P., Green, C. M., Kabengi, N. J., & Hamers, R. J. (2019). Interaction of Phosphate with Lithium Cobalt Oxide Nanoparticles: A Combined Spectroscopic and Calorimetric Study. *Langmuir*, *35*(50), 16640–16649. https://doi.org/10.1021/acs.langmuir.9b02708

Li, X., Volrath, S. L., Nicholl, D. B. C., Chilcott, C. E., Johnson, M. A., Ward, E. R., & Law, M. D. (2003). Development of Protoporphyrinogen Oxidase as an Efficient Selection Marker for Agrobacterium tumefaciens-Mediated Transformation of Maize. *Plant Physiology*, *133*(2), 736–747. https://doi.org/10.1104/pp.103.026245

Lu, Z., Wang, H., Kong, D., Yan, K., Hsu, P., Zheng, G., & Yao, H. (2014). Electrochemical tuning of layered lithium transition metal oxides for improvement of oxygen evolution reaction. *Nature Communications*, *5*, 1–7. https://doi.org/10.1038/ncomms5345

Machado, M. D., & Soares, E. V. (2014). Modification of cell volume and proliferative capacity of Pseudokirchneriella subcapitata cells exposed to metal stress. *Aquatic Toxicology*, *147*, 1–6. https://doi.org/10.1016/j.aquatox.2013.11.017

Machado, M. D., & Soares, E. V. (2020). Reproductive cycle progression arrest and modification of cell morphology (shape and biovolume) in the alga Pseudokirchneriella subcapitata exposed to metolachlor. *Aquatic Toxicology*, *222*(December 2019), 105449. https://doi.org/10.1016/j.aquatox.2020.105449

Malina, T., Maršálková, E., Holá, K., Tuček, J., Scheibe, M., Zbořil, R., & Maršálek, B. (2019). Toxicity of graphene oxide against algae and cyanobacteria: Nanoblade-morphology-induced mechanical injury and self-protection mechanism. *Carbon*, *155*, 386–396. https://doi.org/10.1016/j.carbon.2019.08.086

Melby, E. S., Cui, Y., Borgatta, J., Mensch, A. C., Hang, M. N., Chrisler, W. B., … Orr, G. (2018). Impact of lithiated cobalt oxide and phosphate nanoparticles on rainbow trout gill epithelial cells. *Nanotoxicology*, *12*(10), 1166–1181. https://doi.org/10.1080/17435390.2018.1508785

Mensch, A. C., Mitchell, H. D., Markillie, L. M., Laudadio, E. D., Hedlund Orbeck, J. K., Dohnalkova, A., … Orr, G. (2020). Subtoxic dose of lithium cobalt oxide nanosheets impacts critical molecular pathways in trout gill epithelial cells.

Environmental Science: Nano, *7*(11), 3419–3430. https://doi.org/10.1039/d0en00844c

Moura, I., Moura, J. J. G., Münck, E., Papaefthymiou, V., & LeGall, J. (1986). Evidence for the Formation of a CoFe3S4 Cluster in Desulfovibrio gigas Ferredoxin II. *Journal of the American Chemical Society*, *108*(2), 349–351. https://doi.org/10.1021/ja00262a057

Murphy, L. (2017). THE ELECTRIFYING PROBLEM OF USED LITHIUM ION BATTERIES: RECOMMENDATIONS FOR LITHIUM ION BATTERY RECYCLING AND DISPOSAL, (December).

Niemuth, N. J., Curtis, B. J., Hang, M. N., Gallagher, M. J., Fairbrother, D. H., Hamers, R. J., & Klaper, R. D. (2019). Next-Generation Complex Metal Oxide Nanomaterials Negatively Impact Growth and Development in the Benthic Invertebrate Chironomus riparius upon Settling. *Environmental Science and Technology*, *53*(7), 3860–3870. https://doi.org/10.1021/acs.est.8b06804

Niemuth, N. J., Curtis, B. J., Laudadio, E. D., Sostare, E., Bennett, E. A., Neureuther, N. J., … Klaper, R. D. (2021). Energy Starvation in Daphnia magna from Exposure to a Lithium Cobalt Oxide Nanomaterial. *Chemical Research in Toxicology*. https://doi.org/10.1021/acs.chemrestox.1c00189

Niemuth, N. J., Zhang, Y., Mohaimani, A. A., Schmoldt, A., Laudadio, E. D., Hamers, R. J., & Klaper, R. D. (2020). Protein Fe-S Centers as a Molecular Target of Toxicity of a Complex Transition Metal Oxide Nanomaterial with Downstream Impacts on Metabolism and Growth. *Environmental Science and Technology*, *54*(23), 15257–

15266. https://doi.org/10.1021/acs.est.0c04779

Nitta, N., Wu, F., Lee, J. T., & Yushin, G. (2015). Li-ion battery materials: present and future. *Biochemical Pharmacology*, *18*(5), 252–264. https://doi.org/10.1016/j.mattod.2014.10.040

OECD. (2011). Test No. 201: Freshwater Alga and Cyanobacteria, Growth Inhibition Test. Organization for Economic Cooperation and Development. OECD Guidelines for Testing of Chemicals, Section 2. OECD Publishing Service, Paris, France. https://doi.org/https://doi. org/10.1787/9789264069923

Prasad, R., Gupta, S. K., Shabnam, N., Oliveira, C. Y. B., Nema, A. K., Ansari, F. A., & Bux, F. (2021). Role of microalgae in global co2 sequestration: Physiological mechanism, recent development, challenges, and future prospective. *MDPI*, *13*(23). https://doi.org/10.3390/su132313061

R Core Team. (2019). R: A Language and Environment for Statistical Computing. Vienna, Austria.

Ritz, C., & Strebig, J. C. (2016). Package “drc”: Analysis of Dose-Response Curves. *R Project*, 149. Retrieved from https://cran.r-project.org/web/packages/drc/drc.pdf

RStudio Team. (2020). RStudio: Integrated Development Environment for R. Boston, MA.

Samimi, S., Maghsoudnia, N., Eftekhari, R. B., & Dorkoosh, F. (2018). *Lipid-Based Nanoparticles for Drug Delivery Systems*. *Characterization and Biology of Nanomaterials for Drug Delivery: Nanoscience and Nanotechnology in Drug*

Delivery. Elsevier Inc. https://doi.org/10.1016/B978-0-12-814031-4.00003-9

Saxena, P., & Harish. (2018). Nanoecotoxicological Reports of Engineered Metal Oxide Nanoparticles on Algae. *Current Pollution Reports*, *4*(2), 128–142. https://doi.org/10.1007/s40726-018-0088-6

Sayers, M. J., Fahnenstiel, G. L., Shuchman, R. A., & Bosse, K. R. (2021). A new method to estimate global freshwater phytoplankton carbon fixation using satellite remote sensing: initial results. *International Journal of Remote Sensing*, *42*(10), 3708–3730. https://doi.org/10.1080/01431161.2021.1880661

Stirling, D. R., Swain-Bowden, M. J., Lucas, A. M., Carpenter, A. E., Cimini, B. A., & Goodman, A. (2021). CellProfiler 4: improvements in speed, utility and usability. *BMC Bioinformatics*, *22*(1), 1–11. https://doi.org/10.1186/s12859-021-04344-9

Sun, J., & Liu, D. (2003). Geometric models for calculating cell biovolume and surface area for phytoplankton. *Journal of Plankton Research*, *25*(11), 1331–1346. https://doi.org/10.1093/plankt/fbg096

U.S. Environmental Protection Agency. (2012). Ecological Effects Test Guidelines OCSPP 850.4500: Algal Toxicity. Office of Chemical Safety and Pollution Prevention; Washington, D.C. (EPA-712C-006. *United States Environmental Protection Agency (USEPA)*, (January), 26.

Vieira, E. M., Sarmento, H., Rocha, O., & Seleghim, M. H. R. (2017). Effects of diuron and carbofuran and their mixtures on the microalgae Raphidocelis subcapitata. *Ecotoxicology and Environmental Safety*, *142*(November 2016), 312–321. https://doi.org/10.1016/j.ecoenv.2017.04.024

Wang, F., Guan, W., Xu, L., Ding, Z., Ma, H., Ma, A., & Terry, N. (2019). Effects of Nanoparticles on Algae: Adsorption, Distribution, Ecotoxicity and Fate. https://doi.org/10.3390/app9081534

Yaakob, M. A., Mohamed, R. M. S. R., Al-Gheethi, A., Ravishankar, G. A., & Ambati, R. R. (2021). Influence of nitrogen and phosphorus on microalgal growth, biomass, lipid, and fatty acid production: An overview. *Cells*, *10*(2), 1–19. https://doi.org/10.3390/cells10020393

Yan, N., & Wang, W. X. (2021). Novel Imaging of Silver Nanoparticle Uptake by a Unicellular Alga and Trophic Transfer to Daphnia magna. *Environmental Science and Technology*, *55*(8), 5143–5151. https://doi.org/10.1021/acs.est.0c08588

Zhang, C., Chen, X., Chou, W. C., & Ho, S. H. (2021). Phytotoxic effect and molecular mechanism induced by nanodiamonds towards aquatic Chlorella pyrenoidosa by integrating regular and transcriptomic analyses. *Chemosphere*, *270*, 129473. https://doi.org/10.1016/j.chemosphere.2020.129473

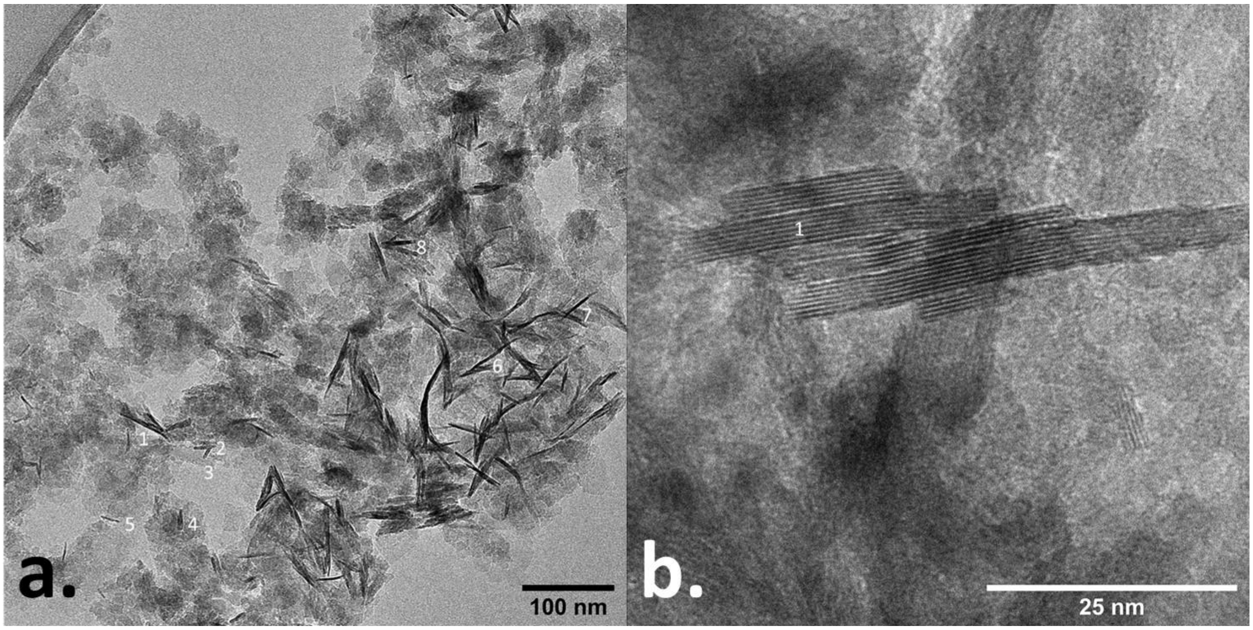

Figure 1 TEM image displaying different size distributions of LCO nanoparticles.

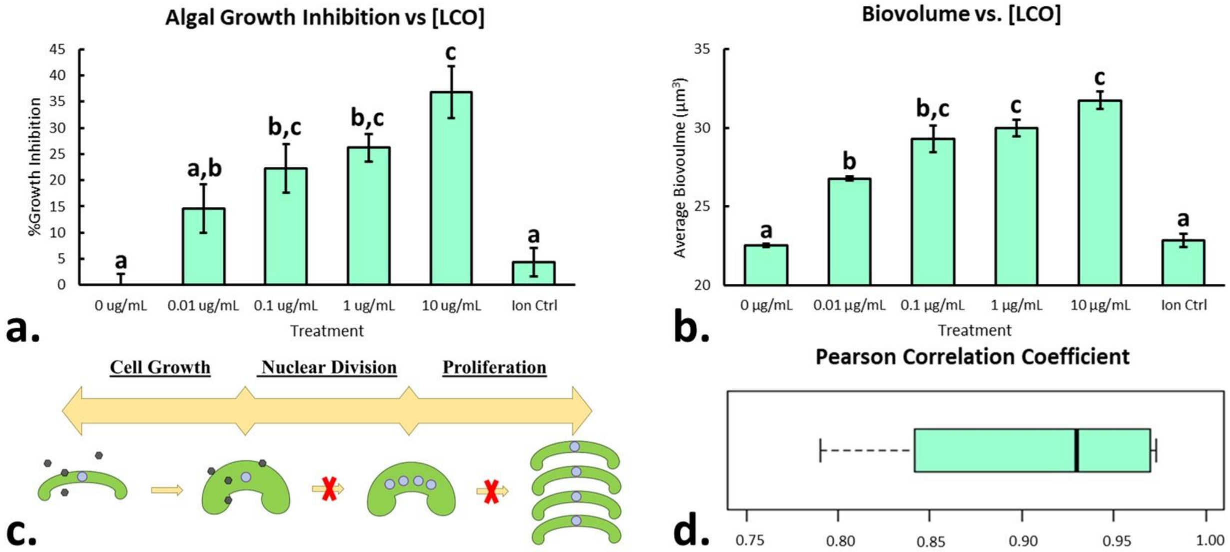

Figure 2: (a.) Algal growth inhibition and (b.) average biovolume in response to varying concentrations of LCO after 48 hours of exposure. Significant differences were determined using a one-way ANOVA with a Tukey post-hoc for multiple comparisons; columns with different letters differ significantly ($p<0.05$). Error bars represent SEM. (c.) Simplified diagram of interrupted *R. subcapitata* cell cycle when exposed to LCO. (d.) Pearson coefficient correlation between algal growth inhibition and average biovolume across four replicates.

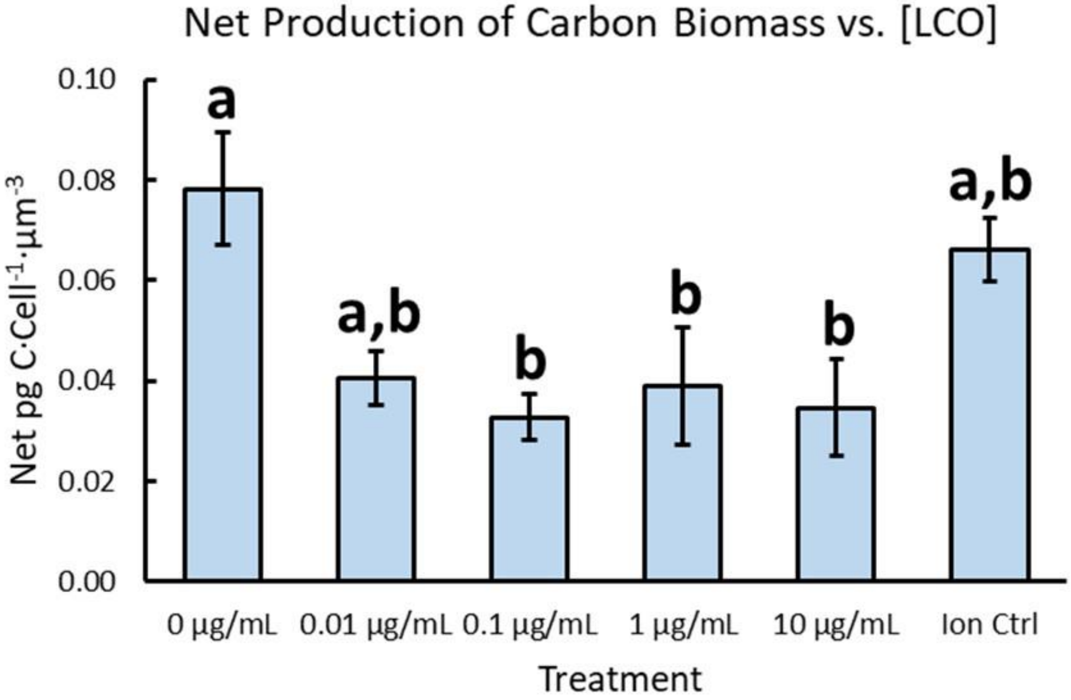

Figure 3: Net production of carbon biomass in response to varying concentrations of LCO after 48 hours of exposure. Significant differences were determined using a one-way ANOVA with a Tukey post-hoc for multiple comparisons; columns with different letters differ significantly ($p<0.05$). Error bars represent SEM.

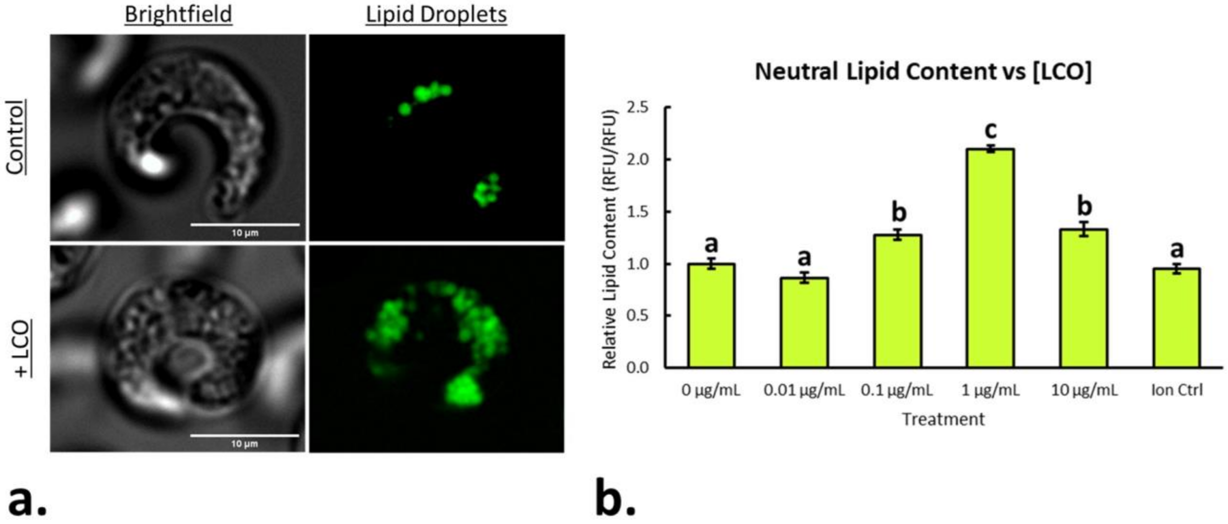

Figure 4: (a.) Representative fluorescence micrograph of a control cell (top) and an LCO-treated cell (bottom, 1 $\mu g \cdot mL^{-1}$). (b.) Relative neutral lipid content in response to varying concentrations of LCO after 48 hours of exposure. Significant differences were determined using a one-way ANOVA with a Tukey post-hoc for multiple comparisons; columns with different letters differ significantly ($p<0.05$). Error bars represent SEM.

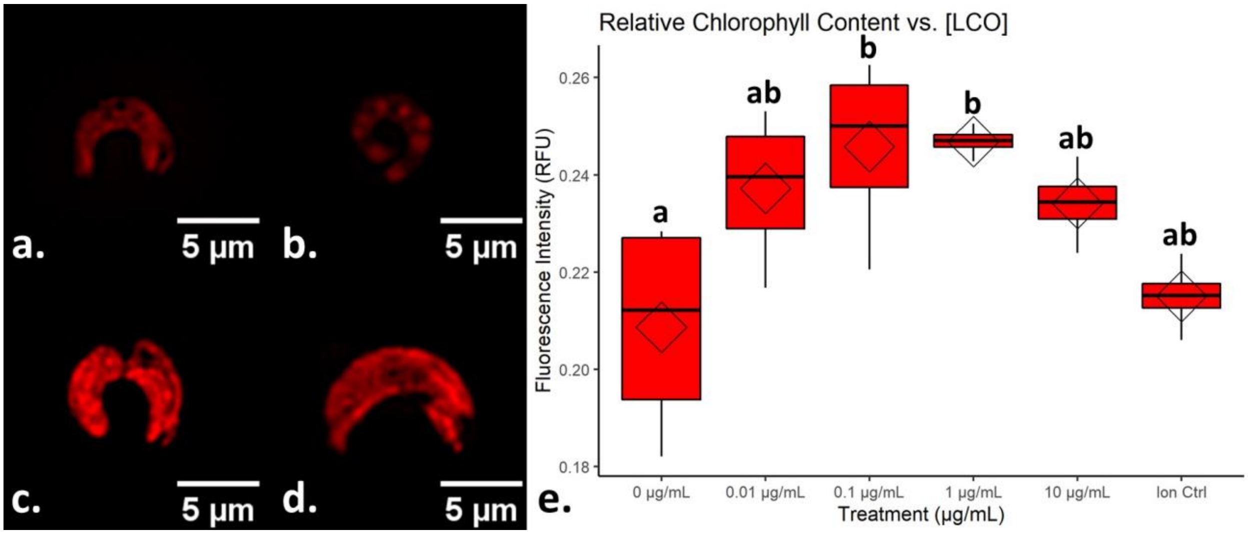

Figure 5: Representative fluorescence micrograph of (a.) a control cell, (b.) a Carfentrazone-treated cell used as a positive control for membrane damage, and an LCO-treated cell exposed to (c.) 1 μg·mL^{-1} LCO and (d.) 10 μg·mL^{-1} LCO. (e.) Relative chlorophyll content in response to varying concentrations of LCO after 48 hours. Bars on boxplots represent treatment medians while diamonds represent treatment averages. Significant differences were determined using a one-way ANOVA with a Tukey post-hoc for multiple comparisons; columns with different letters differ significantly (p<0.05).

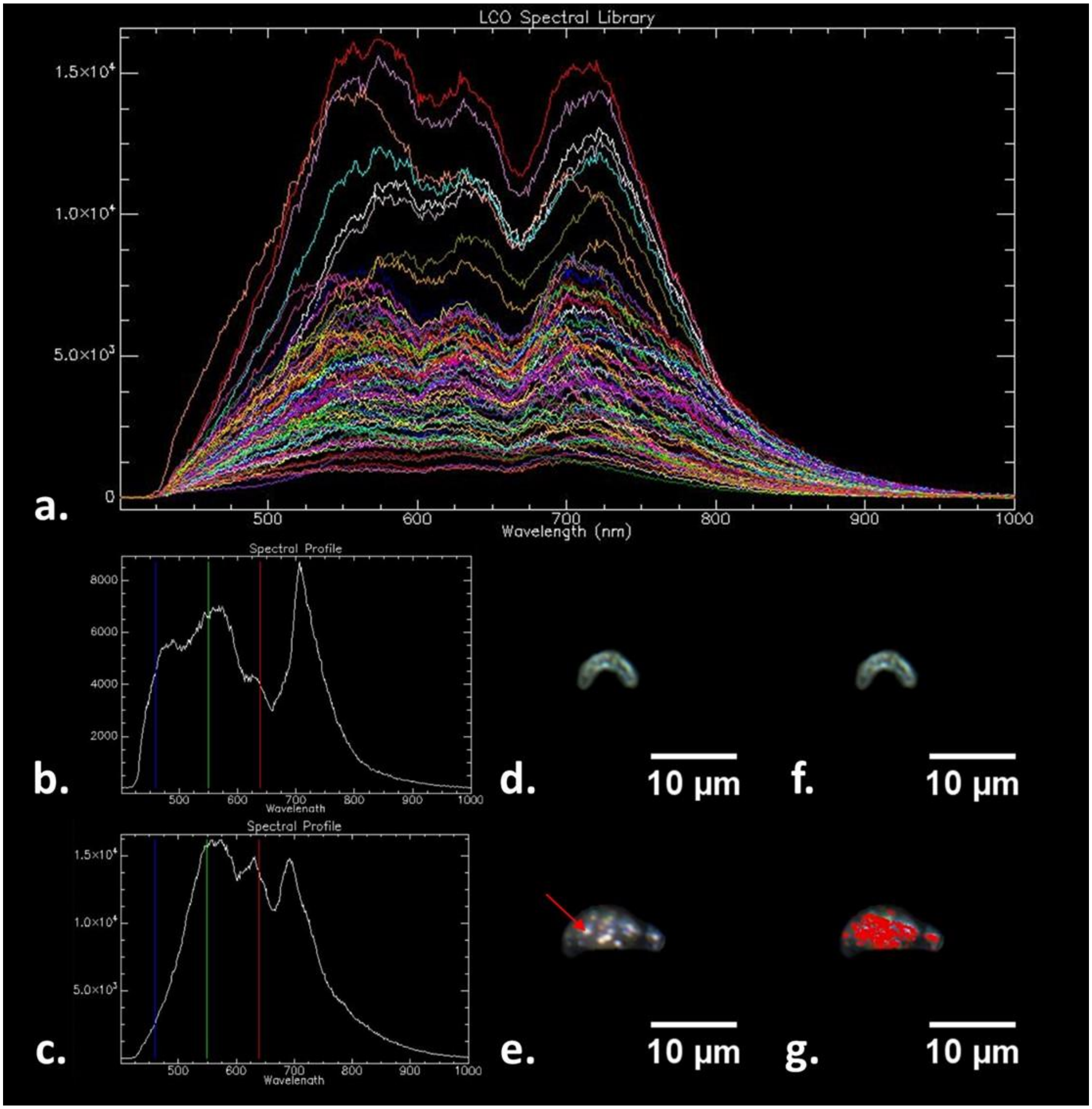

Figure 6: (a.) Reference LCO spectra library. Spectra generated by (b.) a control cell and (c.) an internalized LCO-deposit from a cell exposed to 1 µg·mL^{-1} LCO. Representative darkfield micrograph of (d.) a control cell and (e.) a cell exposed to 1 µg·mL^{-1} LCO; the red arrow points to an internalized LCO deposit. Representation of the spectral angle mapping algorithm used to identify pixels matching the LCO spectra library in (f.) a control cell and (f.) a cell exposed to 1 µg·mL^{-1} LCO; pixels matching the LCO spectra library are mapped in red.